Applied Catalysis B: Environmental 178 (2015) 201–209

Contents lists available at ScienceDirect

Applied Catalysis B: Environmental

journal homepage: www.elsevier.com/locate/apcatb

Hysteresis phenomena and rate fluctuations under conditions of glycerol photo-reforming reaction over CuO_x/TiO_2 catalysts

Athanasia Petala [a], Evangelia Ioannidou [a], Aglaia Georgaka [b], Kyriakos Bourikas [b], Dimitris I. Kondarides [a,*]

[a] Department of Chemical Engineering, University of Patras, GR-26504 Patras, Greece
[b] School of Science and Technology, Hellenic Open University, GR-26222 Patras, Greece

ARTICLE INFO

Article history:
Received 18 July 2014
Received in revised form 6 September 2014
Accepted 8 September 2014
Available online 16 September 2014

Keywords:
Hydrogen
Glycerol
Photo-reforming
Copper oxide
TiO_2
Hysteresis
Oscillations

ABSTRACT

The production of hydrogen by photocatalytic reforming of aqueous solutions of glycerol has been investigated over CuO_x/TiO_2 catalysts of variable metal loading (0.01–2.8 wt.% Cu) prepared by the equilibrium deposition filtration (EDF) method. It has been found that the EDF method results in the formation of highly dispersed copper(II) species, which interact strongly with the TiO_2 surface and retain their characteristics upon heating at temperatures of 450 °C. Results of photocatalytic performance tests obtained under simulated solar light irradiation show that glycerol is photo-reformed efficiently over CuO_x/TiO_2 catalysts toward H_2 and CO_2 with intermediate formation of acetone, acetaldehyde and formic acid. The rate of hydrogen production increases significantly with increase of Cu loading from 0.01 to *ca.* 1.0 wt.% Cu and is enhanced by a factor of 10 with increase of initial glycerol concentration from 0.37 mM to 1 M. Results obtained with the use of low initial glycerol concentrations in solution show that CO_2 evolves in the gas phase immediately after illumination whereas production of H_2 exhibits a hysteresis and appears at the reactor effluent only after prolonged exposure to light. Under these conditions, the rates of both H_2 and CO_2 production were found to "fluctuate" with irradiation time. This behavior has been attributed to the light-induced periodic change of the oxidation state of deposited copper species and the different reactivity of these species for H_2 and CO_2 evolution. To our knowledge, this is the first example of a photocatalytic system that exhibits such dynamic characteristics.

1. Introduction

Development of efficient and stable solar light-responsive semiconductor photocatalysts has been the subject of intensive investigation in recent years [1–4] because of the potential use of these materials in several environmental and energy related applications, including production of "solar" hydrogen by photo(electro)catalytic splitting of water [5–9] and photo-reforming of organic compounds in solution [9–17]. Titanium dioxide (TiO_2), despite its relatively wide band gap ($E_{bg} \approx 3.2$ eV), remains the catalyst of choice in most studies because of its favorable flat band potential and high (photo)chemical stability [18]. In particulate systems, the efficiency of TiO_2 for hydrogen production is enhanced significantly following deposition of small amounts of platinum (or other noble metals) on the semiconductor surface [10–15], because of the well-known ability of dispersed Pt crystallites to retard the rate of recombination of photogenerated charge carriers and to reduce the overpotential for H_2 evolution [9,19–22]. The high cost and the relatively low availability of Pt are strong limitations for its use in large scale applications [23]. Therefore, several transition metals have been investigated as alternative co-catalysts, including Ni and Cu [24], which are largely available and of low cost. Among these, copper is a promising candidate, because it has been shown to facilitate the separation of photogenerated carriers and to reduce the effective band gap of TiO_2 by creating defect and *d*-band states in TiO_2 [23,25,26].

The two stable copper oxides, namely cupric oxide (CuO, $E_{bg} = 1.4$ eV) and cuprous oxide (Cu_2O, $E_{bg} = 2.2$ eV), are direct band gap, *p*-type semiconductors due to the presence of copper vacancies in their structure [27,28]. Although these materials have a high absorption coefficient and can be excited by visible light, they are considered to be inefficient photocatalysts because they are subject to photo-corrosion when exposed to light [29]. However, it has been reported that the stability of copper oxides (CuO_x) can be improved

* Corresponding author. Tel.: +30 2610969527; fax: +30 2610991527.
E-mail address: dimi@chemeng.upatras.gr (D.I. Kondarides).

http://dx.doi.org/10.1016/j.apcatb.2014.09.021
0926-3373/

when coupled with other materials, such as TiO_2 [30,31]. Copper-promoted TiO_2 photocatalysts have been found to be active for the photocatalytic degradation of organic compounds in aqueous media [32–37] and to promote the production of H_2 by providing active sites for H_2 evolution [23,24,31,38–42]. Interestingly, it has been reported that Cu shows only slightly weaker enhancement of TiO_2 activity for hydrogen generation, compared to noble metals, such as Pt, Au, and Pd [43,44]. The above properties, and the fact that both copper and titanium are in relatively large abundance in the Earth's crust, give promise that these materials could be used for large scale solar energy conversion technologies [45].

In addition to their photocatalytic properties and their potential use for other functional applications [46–48], supported copper and copper oxides are known to be effective classical (thermal) catalysts for several reactions, including selective reduction of NO [49], decomposition of N_2O [50], oxidation of CO [51], oxidation of ethanol [52], etc. Depending on the reaction under consideration and the experimental conditions employed, the active phase has been reported to be metallic Cu [53,54], Cu_2O [55], nanosize forms of surface Cu^{2+} ions [56] or a mixture of CuO_x species [50,57–60]. A very interesting characteristic of copper-catalyzed reactions is that the reaction rate and/or the selectivity to reaction products often exhibit an oscillating behavior. Examples of such reactions include oxidation of hydrogen [61], carbon monoxide [62], propene [57], ethanol [61] and volatile organic compounds [63], selective oxidation of methanol to formaldehyde [58], decomposition of N_2O [55,64], and oxidation of sulfur compounds by peroxide in aqueous solutions [65]. In most cases, oscillations have been discussed in the framework of a phase transition between metallic copper and copper oxides and were attributed to the different reactivity of these species [57,58]. In addition to oscillations, the activity and selectivity of copper catalysts often show hysteresis. This has been the case, for example, for the oxidation of hydrogen [66], the oxidative dehydrogenation of methanol to formaldehyde [54,59,67] and the oxidation of propylene to acrolein [68].

The aim of the present work is to investigate the performance of CuO_x/TiO_2 photocatalyst suspensions, irradiated with a solar light-simulating source, for the production of hydrogen via the glycerol photo-reforming reaction. Deposition of copper on the semiconductor surface has been achieved employing the equilibrium deposition filtration (EDF) method [69], which allows the formation of well dispersed CuO_x species under controlled synthesis conditions. The effects of copper loading and glycerol concentration on photocatalytic performance have been investigated in a systematic manner in order to explain the rate fluctuations and hysteresis phenomena observed under certain experimental conditions.

2. Experimental

2.1. Catalyst preparation

Copper-promoted TiO_2 photocatalysts of variable metal loading (0.01–2.8 wt.% Cu) were prepared employing the equilibrium deposition filtration (EDF) method [69] using titanium dioxide powder (Degussa P25, 80% anatase–20% rutile, 50 $m^2 g^{-1}$) and $Cu(NO_3)_2{\cdot}2.5H_2O$ (98%, Aldrich) as the metal precursor salt. A thermostated vessel equipped with a pH control system and a dosimeter have been used. The pH control system allowed the automatic adjustment of the pH during the preparation by adding to the preparation vessel KOH 0.1 M aqueous solution. Nitrogen was bubbled into the vessel during the preparation to prevent the dilution of the atmospheric CO_2, which would bring about a change in the pH. For the preparation, a certain volume of copper nitrate solution of various concentrations in the range 10^{-3} to 5×10^{-3} M was used (depending on the sample). The ionic strength of these solutions was adjusted at 0.1 M by using KNO_3 and the initial pH was adjusted in a constant value, in the range 3–6. A given amount of the titania powder was added into the stirred solution. As the deposition of the $Cu(H_2O)_6^{2+}$ ions caused a decrease in pH, the pH control system fed the solution with a suitable amount of the KOH solution to keep pH at its initial value. When the pH control system stopped to feed KOH solution, the suspension was filtered. The Cu(II) concentration in the solid was determined by measuring photometrically (λ = 603 nm) its concentration in the corresponding impregnating solution before and after deposition using a Lamda-35 UV–Vis, Perkin Elmer spectrophotometer. The obtained solids were either only dried at 110 °C for 4 h or subsequently calcined in air at 450 °C for 2.5 h, and are denoted in the following as *x*Cu(D) (dried samples) or *x*Cu(C) (calcined samples), where *x* represents the copper loading (wt.%). In Table 1 are listed the photocatalyst samples prepared in this study together with the synthesis conditions employed.

2.2. Catalyst characterization

The synthesized materials were characterized with respect to their specific area, phase composition and light absorption properties, employing nitrogen physisorption at the temperature of liquid nitrogen (BET), X-ray diffraction (XRD), and UV–vis-NIR spectroscopy. Measurements of SSA were obtained with the use of a Micromeritics Gemini V apparatus. The XRD patterns were obtained using a Brucker D8 Advance instrument employing Cu Kα source (λ = 1.5496 Å) operated at 40 kV and 40 mA. Data were collected in the 2θ range of 2–85° at a scan rate of 0.05° s^{-1} and a step size of 0.015°. The anatase content of TiO_2 (x_A) was estimated using the following equation [70]:

$$x_A = \left[1 + 1.26\left(\frac{I_R}{I_A}\right)\right]^{-1} \quad (1)$$

where I_A and I_R are the intensities of the anatase (1 0 1) and rutile (1 1 0) reflections, respectively. The primary crystallite size of nanocrystals was estimated by means of the Debye-Scherrer's formula [71].

The UV–Vis-NIR spectra were recorded on a Lamda-35, PerkinElmer spectrophotometer equipped with an integration sphere, using either TiO_2(P25) or $BaSO_4$ as a reference.

2.3. Photocatalytic performance tests

The experimental setup used for the assessment of photocatalytic activity of CuO_x/TiO_2 samples for the title reaction comprises a solar light-simulating source, a quartz photoreactor and an on-line analysis system [12–14]. The lamp housing (Oriel) is furnished with a Xe arc lamp (Osram 300 W), a set of lenses for light collection and focusing, and a water filter for the elimination of infrared radiation. For the experiments reported here, the lamp power was set at 250 W and the photon flow entering the reactor, measured by chemical actinometry [72], was found to be 3.8×10^{-7} Einsteins s^{-1}.

The quartz photoreactor is of cubic shape with flat windows (40 mm × 40 mm) and a top cover, which is connected to the cell via an NS40 joint. The top cover has provisions for inlet/outlet of an inert gas (Ar) that flows through the suspension and serves as a means of collecting gaseous reaction products and carrying them into the on-line analysis system. The gas inlet terminates in a fritted glass section though which the carrier gas is effectively dispersed into the suspension. The gas outlet is equipped with a water-cooled condenser, which does not allow vapours to escape the reactor. The headspace of the reactor, including the volume of tubing up to the analysis system, is *ca.* 250 cm^3.

Table 1
Photocatalyst samples and synthesis conditions.

Photoatalyst sample notation	Copper loading (wt.%)	Synthesis conditions		
		pH	Cu(II) concentration (mol L^{-1})	Heat treatment
TiO_2	–	–	–	–
0.01Cu(D)	0.01	3.0	10^{-3}	110 °C
0.01Cu(C)				450 °C
0.04Cu(D)	0.04	4.0	10^{-3}	110 °C
0.04Cu(C)				450 °C
0.18Cu(D)	0.18	4.5	10^{-3}	110 °C
0.18Cu(C)				450 °C
0.29Cu(D)	0.29	5.0	10^{-3}	110 °C
0.29Cu(C)				450 °C
0.4Cu(D)	0.4	6.0	10^{-3}	110 °C
0.4Cu(C)				450 °C
0.9Cu(D)	0.9	6.0	2×10^{-3}	110 °C
0.9Cu(C)				450 °C
1.5Cu(D)	1.5	6.0	3×10^{-3}	110 °C
1.5Cu(C)				450 °C
2.1Cu(D)	2.1	6.0	4×10^{-3}	110 °C
2.1Cu(C)				450 °C
2.8Cu(D)	2.8	6.0	5×10^{-3}	110 °C
2.8Cu(C)				450 °C

The on-line analysis system comprises a gas chromatograph (Varian 3800), equipped with a molecular sieve 5A column and a TCD detector, and an infrared analyzer (BINOS) that allow continuous monitoring of H_2 and CO_2, respectively. The GC is interfaced to a personal computer, which enables automatic sampling of the gas exiting from the reactor at pre-selected time intervals via an electrically actuated gas sampling valve.

In a typical experiment, a known amount of photocatalyst (80 mg) in powder form ($d < 90$ μm) is dispersed in triply distilled water (60 mL) under continuous stirring, followed by addition of glycerol. The top cover is then put in place, the cell is purged with flowing Ar to remove atmospheric oxygen from the reactor and tubing, and the reactor is exposed to light (at $t = 0$) under continuous stirring. All experiments reported here were carried out at room temperature under a constant Ar flow of 20 cm^3 min^{-1}.

Identification and quantification of reaction intermediates in the liquid phase has been achieved in separate experiments where the reaction was stopped at the desired irradiation time, the suspension was collected, filtered and stored in sealed vials in a refrigerator. Analysis was performed with the use of a gas chromatography–mass spectrometry (GC/MS) system [73,74]. Identification of the GC/MS spectral features has been achieved with the use of a built-in library. Response factors were determined with the use of self-prepared solutions of known concentration.

3. Results and discussion

3.1. Photocatalyst characterization

Typical XRD patterns obtained for pristine TiO_2(P25) and for two samples with relatively high Cu loadings calcined at 450 °C, namely 1.5Cu(C) and 2.8Cu(C), are shown in Fig. 1. It is observed that the Cu-loaded samples (traces b and c) display the typical diffraction pattern of TiO_2(P25) (trace a), which is characterized by peaks attributed to anatase and rutile phases. Similar results were obtained for all materials synthesized in the present work. The absence of diffraction peaks corresponding to CuO_x phases implies a good dispersion of the deposited copper species. Results of BET and XRD measurements showed that the synthesized *x*Cu(D) and *x*Cu(C) catalysts have, practically, the same specific surface area

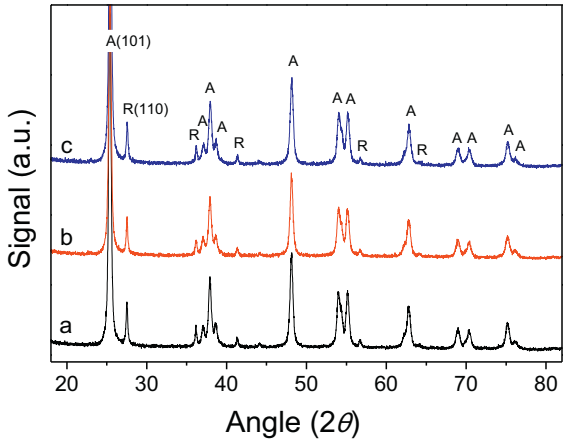

Fig. 1. Representative X-ray diffraction patterns obtained over (a) pristine TiO_2(P25), (b) 1.5Cu(C) and (c) 2.8Cu(C) photocatalysts. Diffraction peaks denoted as "A", and "R" correspond to reflections from the anatase and rutile phases of TiO_2, respectively.

(45 ± 2 m^2/g), anatase content (ca. 87 ± 1%) and primary crystallite size (22.5 ± 0.7 nm for anatase and 37.9 ± 2.7 nm for rutile) with the parent TiO_2 material.

3.2. Optical properties

The evolution of the structure of the copper species formed on the TiO_2 surface at the various steps of the preparation procedure was followed with UV–vis-NIR spectroscopy. Typical results obtained during the synthesis of the 0.29Cu/TiO_2 samples are presented in Fig. 2, which shows the absorbance spectrum of the initial solution (trace a) and the diffuse reflectance (DR) spectra of the as-prepared (trace b), dried (trace c) and calcined (trace d) Cu-loaded powders. It should be noted that the DR spectra (traces b–d) were recorded using TiO_2 as reference in order to discriminate the absorption bands originating from the deposited copper species. It is observed that the spectrum of the aqueous $[Cu(H_2O)_6]^{2+}$ solution exhibits a broad absorption band at wavelengths longer than 600 nm, which is centered at *ca.* 810 nm (trace a). This band can be

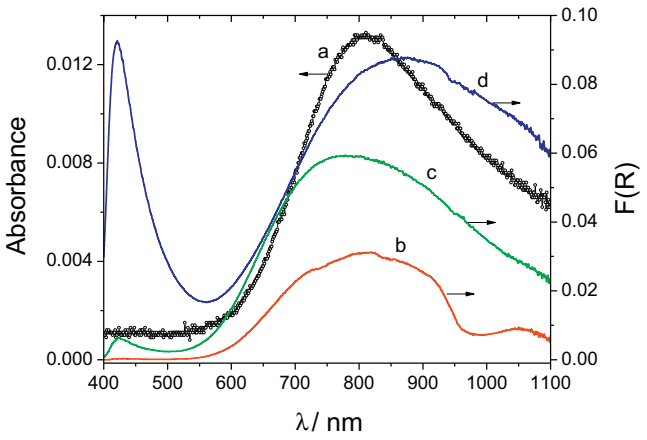

Fig. 2. UV–vis-NIR spectra obtained at various steps of the synthesis of 0.29Cu/TiO_2 photocatalysts: (a) absorbance of an aqueous solution of $[Cu(H_2O)_6]^{2+}$ species (Cu(II) concentration: 0.001 M, pH 5, ionic strength 0.1 M). Diffuse reflectance (DR) spectra of (b) the "wet" sample taken from an EDF experiment just after filtration, comprising $[Cu(H_2O)_6]^{2+}$ ions absorbed on the titania surface; (c) the 0.29Cu(D) catalyst obtained after drying of the wet sample at 110 °C for 4 h; (d) the 0.29(C) catalyst obtained after drying (110 °C for 4 h) and subsequent calcination (450 °C for 2.5 h) of the wet sample. DR spectra were obtained using TiO_2 as reference.

attributed to the *d*–*d* transitions of Cu^{2+} species in an octahedral (O_h) configuration, which are more or less tetragonally distorted [75,76]. The DR spectrum of the "wet" sample, taken from the EDF experiment just after deposition and filtration, exhibits similar absorption characteristics (trace b). More specifically, the spectrum is characterized by a multiple band in the region of 600–950 nm and an additional one located at *ca.* 1050 nm. Similar profiles (not shown for brevity) were obtained for all "wet" samples, in which Cu(II) loading varied in the range 0.01–2.8% (w/w) (Table 1). It is of interest to note that deposition of the $[Cu(H_2O)_6]^{2+}$ ions on the TiO_2 surface (trace b) results in a shift of the absorption band to longer wavelengths, compared to the solution (trace a). Such a shift, which is typical of the presence of some weaker ligand field donors in the coordination sphere of transition metal cations in the deposited octahedral species [77–81], indicates the replacement of one or more aqua ligands with surface oxygen atoms and thus the formation of inner sphere complexes, where Cu(II) remains in octahedral symmetry [77–81].

The DR spectrum obtained after drying of the sample at 110 °C (trace c) is not significantly different, compared to that of the wet sample (trace b), indicating that Cu(II) species do not appear in a new structure or in a different oxidation state. A noticeable difference is the appearance of a new band located at *ca.* 420 nm (trace c), the intensity of which increases significantly upon calcination of the sample at 450 °C (trace d). It is known that the DR spectrum of TiO_2 exhibits a broad band in the range of 200–400 nm, which is attributed to the $O^{2-} \rightarrow Ti^{4+}$ charge transfer process that takes place in the Ti(IV) oxide [82]. This band should not appear in the DR spectra of Fig. 2, because they were recorded using pristine TiO_2 as reference. Therefore, the band at 420 nm may be attributed to interfacial charge transfer from the O 2*p* valence band of TiO_2 to the Cu(II) state of deposited species [26,34,35,56]. This argument is supported by the observation that increase of Cu loading from 0.01% to 2.8% (w/w) results in a monotonic increase of the intensity of the 420-nm band for both *x*Cu(D) (Fig. 3A) and the *x*Cu(C) (Fig. 3B) samples. The fact that the intensity of this band is much higher for the calcined samples indicates that treatment in air at high temperatures enhances the degree of interaction between the deposited Cu(II) species and the TiO_2 surface. It should be mentioned that similar bands have been observed in the DR spectra of several TiO_2-supported transition metal catalysts after drying and/or calcination, attributed to strong interactions developed between the supported phase and the TiO_2 [78,83,84].

The DR spectra of the calcined samples (Fig. 3B) indicate the presence of Cu^{2+} species in O_h coordination (broad band at ~850 nm). Most probably, these species are present as Cu(II) nanoclusters attached to the TiO_2 surface and not as bulk CuO crystallites, the DR spectrum of which is known to be characterized by an intense band centered at *ca.* 650 nm [75,85]. This argument is supported by the results of Li et *al.* [33] who reported that deposited bulk CuO crystallites do not show an absorbance peak at 400–500 nm, which is only displayed when Cu(II) ions are attached to TiO_2. Thus, it may be suggested that the synthesis method employed here (EDF) results in the formation of well dispersed, isolated Cu^{2+} species, which are stable even after calcination at 450 °C. More specifically, and according to preliminary EPR results (not shown here), it may be argued that the copper species deposited on the TiO_2 surface comprise closely spaced, discrete Cu atoms (most likely Cu-Cu dimmers), but not tightly packed, magnetic Cu phases. This argument is supported by the absence of CuO_x reflections in the XRD patterns of Fig. 1.

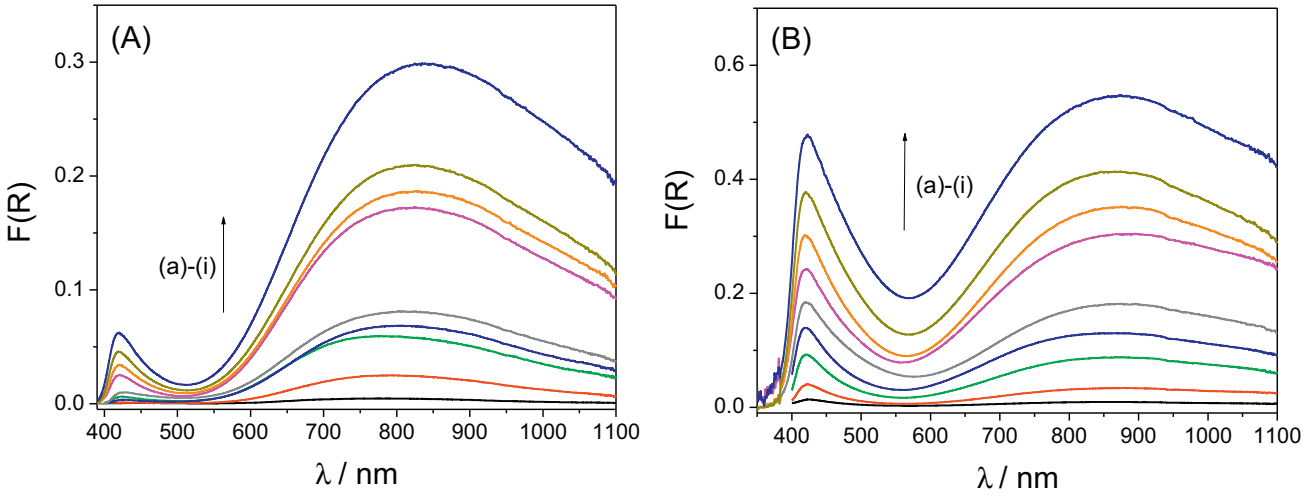

Fig. 3. UV–vis-NIR DR spectra of (A) the *x*Cu(D) photocatalysts obtained after drying of the wet samples at 110 °C for 4 h, and (B) the *x*Cu(C) photocatalysts obtained after drying of the wet samples at 110 °C for 4 h and subsequent calcination at 450 °C for 2.5 h. Cu loading (*x*), (% w/w): (a) 0.01; (b) 0.04; (c) 0.18; (d) 0.29; (e) 0.4; (f) 0.9; (g) 1.5; (h) 2.1; (i) 2.8. All spectra were recorded using TiO_2 as a reference.

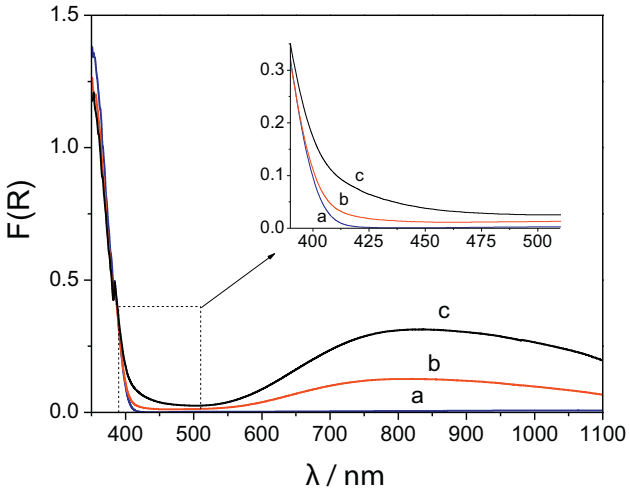

Fig. 4. UV–vis-NIR DR spectra of (a) pristine TiO_2, (b) 0.4Cu(D), and (c) 2.8Cu(D) samples. Spectra were recorded using $BaSO_4$ as a reference.

For comparison purposes, representative DR spectra obtained using $BaSO_4$ as reference are presented in Fig. 4. It is observed that pristine TiO_2 absorbs at wavelengths lower than *ca.* 410 nm (trace a). Deposition of copper results in a shift of the absorption threshold to longer wavelengths (see inset) and extends the absorption of the photocatalyst to the visible and near-infrared region (traces b and c), in agreement with results of previous studies [25,26,33,35,42].

3.3. Hysteresis phenomena and rate fluctuations

Typical results of photocatalytic performance tests obtained over the 0.4Cu(D) photocatalyst suspended in an aqueous glycerol solution (C_{glyc} = 0.37 mM) are presented in Fig. 5A, where the rates of hydrogen (r_{H_2}) and CO_2 (r_{CO_2}) evolution are plotted as functions of irradiation time. Two important observations can be made: first, although CO_2 appears in the gas-phase practically immediately after exposure to light, an induction period (hysteresis) is observed for the evolution of H_2, which is detected in the gas phase after about 1 h under irradiation; second, the rates of both CO_2 and H_2 "fluctuate" with irradiation time exhibiting two maxima, which are more clearly resolved in the case of CO_2. Prolonged exposure to light results in a progressive decrease of both r_{H_2} and r_{CO_2} because of the consumption of organic compounds in solution [12–14]. Qualitatively similar results were obtained with the use of 0.9Cu(C) (Fig. 5B) and other photocatalysts (not shown for brevity).

Although hysteresis and oscillations of reaction rates have been reported for several thermal catalytic reactions (see Section 1), to our knowledge this is the first time that such phenomena are reported for a photocatalytic system. It should be noted that the rate fluctuations reported here have periods of the order of hours (Fig. 5), i.e., much longer than those reported for typical thermal catalytic reactions. This time scale implies that reaction kinetics alone cannot be responsible for this behavior. It is therefore proposed that the driving mechanism for the hysteresis and the rate fluctuations observed in the present work is related to a slow and reversible modification of the oxidation state of dispersed CuO_x species, as discussed below.

The experimental results presented in Fig. 5 can be understood by considering that the glycerol photo-reforming reaction is initiated by excitation of TiO_2 by photons of ultra-band gap energy, which leads to the promotion of electrons in the conduction band (CB) and the formation of holes in the valence band (VB) of the semiconductor:

$$TiO_2 \rightarrow e^-_{CB} + h^+_{VB} \quad (2)$$

In principle, photogenerated CB-electrons (e^-_{CB}) and VB-holes (h^+_{VB}) can react with water (protons) and glycerol to form H_2 and CO_2, respectively, as has been reported for Pt/TiO_2 photocatalysts [12–14]:

$$2H^+ + 2e^-_{CB} \rightarrow H_2 \quad (3)$$

$$C_3H_8O_3 + 3H_2O + 14h^+_{VB} \rightarrow \cdots \rightarrow 3CO_2 + 14H^+ \quad (4)$$

In the present system, however, it is possible that photogenerated carriers may also react with dispersed CuO_x species, which are known to be easily reduced/oxidized by photogenerated electrons/holes of TiO_2 [35,40,86,87]. For instance, Cu_2O may be either reduced to metallic Cu or oxidized to CuO by charge carriers according to [86]:

$$Cu_2O + H_2O + 2e^-_{CB} \rightarrow 2Cu + 2OH^- \quad (5)$$

$$Cu_2O + H_2O + 2h^+_{VB} \rightarrow 2CuO + 2H^+ \quad (6)$$

As shown in the energy diagram of Fig. 6, such reactions are thermodynamically feasible because the band edges of TiO_2 "bracket" the redox potentials of Cu^{2+}/Cu^+, Cu^{2+}/Cu^0 and Cu^+/Cu^0 couples. Returning to Fig. 5A, the observation that CO_2 appears in the gas phase immediately after illumination implies that the photogenerated holes in TiO_2 are consumed to oxidize glycerol according

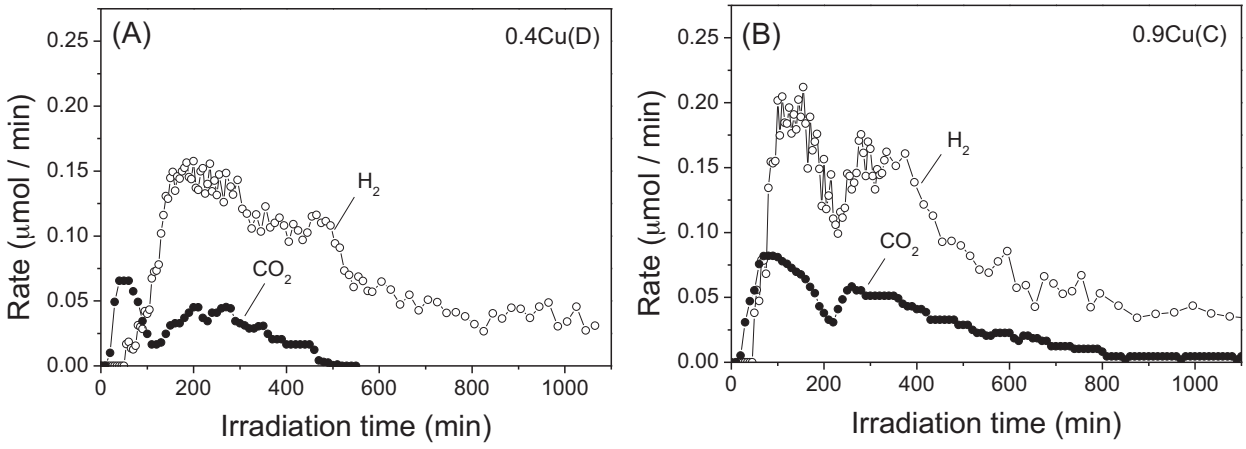

Fig. 5. Rates of H_2 and CO_2 evolution as functions of irradiation time obtained over (A) the 0.4Cu(D) and (B) the 0.9Cu(C) photocatalysts. C_{glyc} = 0.37 mM; C_{cat} = 1.33 g L^{-1}; natural pH.

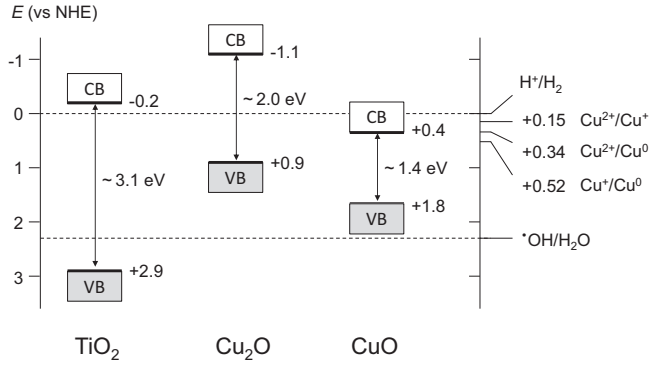

Fig. 6. Schematic diagram showing the positions of the valence band (VB) and conduction band (CB) edges of TiO_2 [88,89], Cu_2O [89–92] and CuO [29,93] semiconductors in contact with aqueous electrolyte at pH0, the redox potentials of copper species and the potential of hydroxyl radical formation. Energies relative to the normal hydrogen electrode (NHE).

to reaction (4) either directly or indirectly via the formation of hydroxyl radicals. In contrast, the relatively long induction period observed for r_{H_2} indicates that, initially, photogenerated electrons in TiO_2 are not consumed for the reduction of protons (Eq. (3)) but for another reaction, which has to be related to the change of the oxidation state of finely dispersed copper species. Results presented in Section 3.2 provide evidence that, before exposure to photo-reaction conditions, copper exists in the Cu(II) state. Since the CB edge of CuO is more positive than that of TiO_2 (Fig. 6), it is expected that photogenerated electrons in TiO_2 will be trapped by Cu(II) to yield Cu(I) (reverse of reaction (6)) and/or metallic Cu (reaction (5)), in agreement with results of previous studies [34,40,41]. The hysteresis observed in the evolution of H_2 may then be explained by considering that reduction of CuO is thermodynamically (Fig. 6) and kinetically more favorable, compared to reduction of protons. As a result, photogenerated electrons are initially consumed mainly for the reduction of dispersed copper species and, therefore, the process does not result in H_2 evolution.

The observation that hydrogen appears in the gas phase only after about 1 h under irradiation, where r_{CO_2} reaches a maximum and then starts to decrease (Fig. 5A) indicates that, at this time period, oxidation of glycerol toward CO_2 by photogenerated holes (Eq. (4)) is suppressed whereas reduction of protons by photogenerated electrons (Eq. (3)) is enhanced. This may be explained by assuming that after about 1 h under irradiation, a critical amount of dispersed CuO species has been reduced toward, for example, Cu_2O. When this happens, Cu_2O starts to reoxidize by h^+_{VB} toward CuO (Eq. (6)) thereby resulting in the suppression of the competitive reaction of glycerol oxidation (Eq. (4)) and the concomitant decrease of r_{CO_2}. At the same time, photogenerated electrons are mainly consumed for the reduction of protons (Eq. (3)) and not for the reduction of CuO thus resulting in a temporary acceleration of the rate of H_2 evolution (Fig. 5A). Further exposure to light results, again, in a progressive increase of the relative amount of CuO, at the expense of that of Cu_2O, and, as a result, the oscillatory cycle starts again. Note that the same reasoning is valid if copper exists on the photocatalyst surface in the form of metallic Cu instead of Cu_2O.

According to the above reaction scenario, exposure of CuO_x/TiO_2 photocatalysts to light under the present reaction conditions results in a periodic change of the oxidation state of dispersed copper species according to [87]:

$$CuO \rightleftarrows Cu_2O \rightleftarrows Cu \quad (7)$$

This periodic change of copper oxidation state leads, in turn, to the observed rate fluctuations because of the different activities of CuO, Cu_2O and/or Cu for the redox reactions that lead to H_2 and CO_2 evolution (Eqs. (3)–(6)). This is in agreement with results of previous studies which reported, for example, that Cu_2O shows a relatively high and stable rate of H_2 evolution whereas r_{H_2} decreases with time over CuO-containing photocatalysts [41].

3.4. Effects of copper loading on photocatalytic performance

Results of photocatalytic performance tests obtained over *x*Cu(D) photocatalysts of variable metal loading (x = 0.04, 0.4, 1.5 and 2.8 wt.% Cu) are summarized in Fig. 7, where the rates of H_2 and CO_2 evolution are plotted as functions of irradiation time. It is observed that increase of copper loading results in a progressive increase of the time period required for the appearance of H_2 in the gas-phase, i.e., from *ca.* 25 min for 0.04Cu(D) to *ca.* 120 min for 2.8Cu(D) (Fig. 7A). This is consistent with the assumption made above that hysteresis is related to reduction of CuO species, which are initially present on the photocatalyst surface. Increase of metal loading from 0.04 to 1.5 wt.% Cu also results in a significant increase of the maximum rate of H_2 evolution, which does not change, practically, upon further increase of copper content to 2.8 wt.% (Fig. 7A). Regarding evolution of CO_2, it is observed that, for all studied samples, r_{CO_2} exhibits two maxima, which increase monotonically in intensity with increase of Cu loading (Fig. 7B). It is of interest to note that evolution of H_2 (Fig. 7A) is initiated only after the appearance of the first rate maximum of CO_2 (Fig. 7B). This indicates that production of H_2 is favored on different sites than those of CO_2, as discussed above.

Similar experiments were performed for all photocatalysts synthesized in this study (not shown for brevity). Results obtained are summarized in Fig. 8, where the maximum rates of H_2 and CO_2 evolution obtained for the dried and the calcined samples are plotted as functions of Cu loading. It is observed that the *x*Cu(D) and *x*Cu(C) samples exhibit a similar performance. In particular, the maximum rate of H_2 evolution increases with increase of Cu loading up to *ca.* 1.0% and then reaches a plateau (Fig. 8A). Regarding CO_2, the rate maximum increases continuously with increase of Cu loading up to 2.8% (Fig. 8B). It is of interest to note that pristine TiO_2 is practically inactive for the title reaction under the present conditions whereas addition of even very small amounts of copper on the photocatalyst surface results in appreciable rates of H_2 and CO_2 evolution (Fig. 8).

Results of previous studies have shown that the photocatalytic performance of CuO_x/TiO_2 catalysts depends strongly on the size and degree of dispersion of copper species [23,24,33,94]. For instance, it has been reported that the activity of CuO_x/TiO_2 catalysts for the degradation of methylene blue is maximized for samples loaded with very small amounts of copper (~0.1 wt.% Cu) [33,94], where copper exists in the form of highly dispersed CuO clusters and/or substitutional Cu^{2+} sites [33]. In contrast, the bulk form of CuO, which is present at higher loadings, was found to result in a decrease of activity [33]. Similarly, Gombac *et al.* [23] concluded that the low initial activity obtained over certain CuO_x/TiO_2 samples under glycerol photo-reforming conditions was due to the presence of large CuO particles that are difficult to be reduced under photo-reaction conditions [23]. The high activity of the copper-loaded TiO_2 catalysts synthesized in the present work by the EDF method may then be attributed to the formation of highly dispersed CuO_x clusters that interact strongly with the TiO_2 surface, as discussed in Section 3.2.

3.5. Effects of initial glycerol concentration

The effects of initial glycerol concentration (C_{glyc}) on photocatalytic activity have been investigated over the 0.4Cu(C) catalyst and results obtained are summarized in Fig. 9. It is observed that increase of C_{glyc} from 0.37 mM to 1 M results in a 10-fold

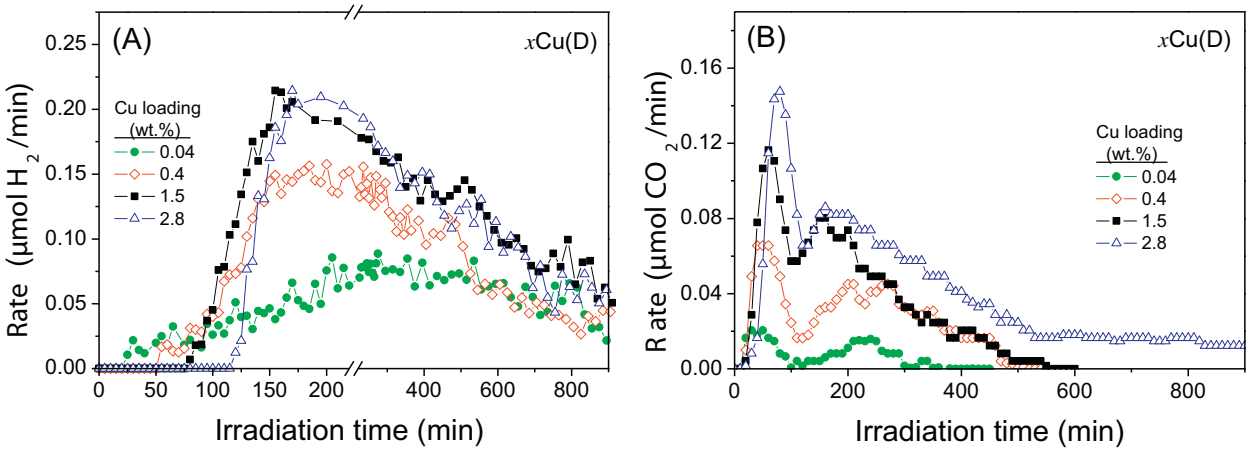

Fig. 7. Rates of (A) H_2 and (B) CO_2 evolution as functions of irradiation time obtained over the *x*Cu(D) photocatalysts of variable copper loading. C_{glyc} = 0.37 mM.

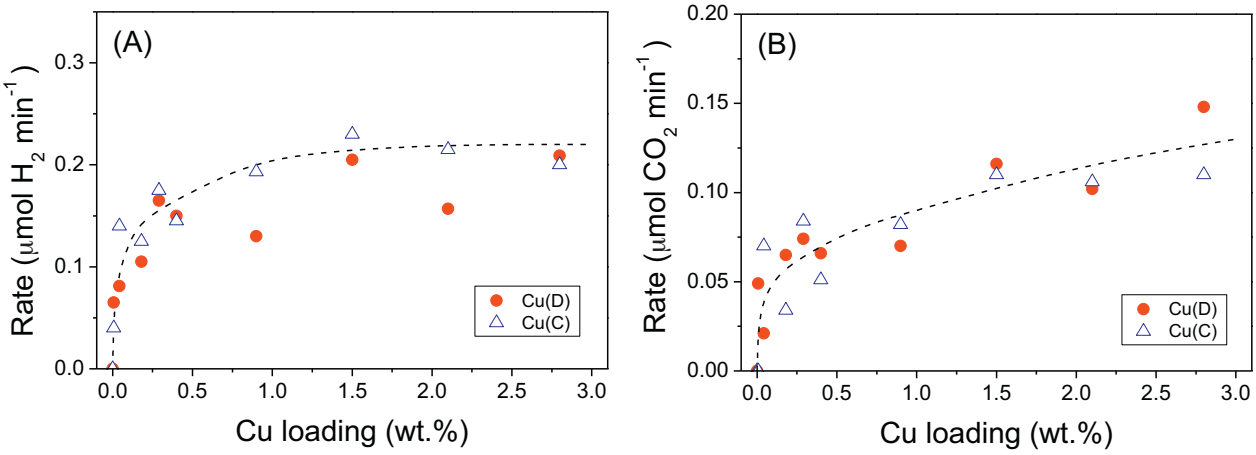

Fig. 8. Maximum rates of (A) H_2 and (B) CO_2 evolution as functions of copper loading obtained over the *x*Cu(D) and *x*Cu(C) photocatalysts. C_{glyc} = 0.37 mM.

increase of the maximum rate of H_2 evolution and in progressively shorter hysteresis periods (Fig. 9A). It is of interest to note that a shoulder appears systematically at irradiation times of *ca.* 60 min in the H_2-rate curves obtained for high glycerol concentrations (traces c–e), which can be related to the rate fluctuations discussed above. Regarding the evolution of CO_2 (Fig. 9B), the rate curves obtained for low glycerol concentrations (traces a and b) are characterized by two rate maxima similar to those shown in Figs. 5 and 7. However, further increase of C_{glyc} results in the disappearance of the first rate maximum (traces c–e). This behavior can be explained by considering that under these conditions ($C_{glyc} \geq 10$ mM), where the surface coverage of glycerol is increased, the photo-induced oxidation reactions do not result, initially, in deep oxidation of glycerol toward CO_2 but to the formation of other

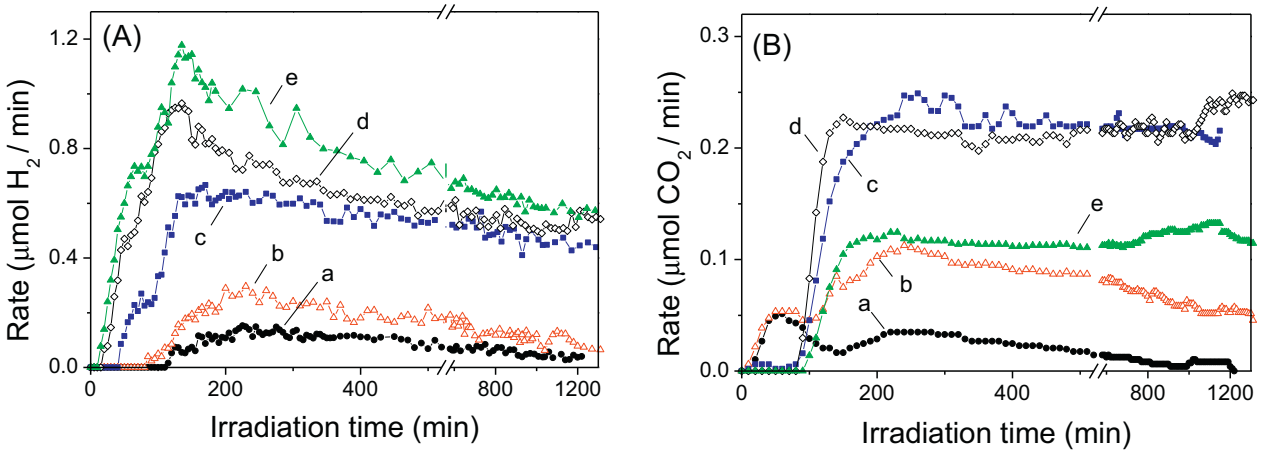

Fig. 9. Rates of (A) H_2 and (B) CO_2 evolution as functions of irradiation time obtained over the 0.4Cu(C) photocatalyst with the use of solution of variable initial glycerol concentration: (a) 0.37 mM; (b) 1.0 mM; (c) 10 mM; (d) 100 mM; (e) 1.0 M.

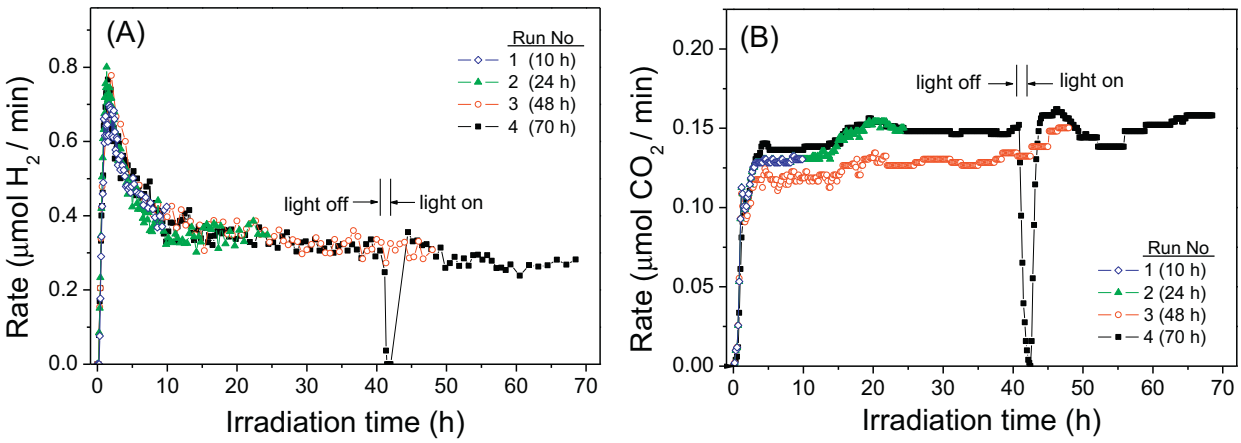

Fig. 10. Rates of (A) H_2 and (B) CO_2 evolution obtained with the use of the 0.9Cu(C) photocatalyst in four different experiments lasted for 10, 24, 48 and 72 h. In the latter experiment, light was switched off at t = 40.5 h for a period of 90 min. C_{glyc} = 100 mM.

intermediate products. This hypothesis is supported by the observation that r_{CO2} reaches a maximum value of *ca.* 0.22 μmol/min for C_{glyc} = 10–100 mM (traces c and d) and decreases significantly to *ca.* 0.12 μmol/min for C_{glyc} = 1 M (trace e). This indicates that selectivity toward CO_2 decreases at high initial glycerol concentrations in agreement with the above assumption.

Inspection of the rate curves presented in Fig. 9 shows that fluctuations of the rates of H_2 and CO_2 evolution are not clearly observed for initial glycerol concentrations higher than 10 mM (traces c–e). This, together with the different method employed here for the synthesis of CuO_x/TiO_2 photocatalysts, may explain the reason why this phenomenon has not been reported in previous studies related to production of H_2 by photo-reforming of organic compounds in solution. On the other hand, an induction period in H_2 evolution may be present in some published results (e.g., [23]), which is not discussed by the authors.

3.6. Identification of reaction intermediates in solution

The evolution of reaction intermediates in the liquid phase has been investigated with the use of the 0.9Cu(C) catalyst and an initial glycerol concentration of 100 mM. For this, the reaction was stopped at the desired irradiation periods, the suspension was collected, filtered and the filtrate was analyzed with GC/MS. In Fig. 10 are shown the rate curves of H_2 and CO_2 evolved in the gas phase for experimental runs that lasted for 10, 24, 48 and 70 h. It is observed that the reproducibility of the measured reaction rates is very good for both gas-phase products. In the same figure it is also shown that when the light was switched off (at t = 40.5 h, run No 4) the rates of both H_2 and CO_2 dropped to zero and returned to their previous values upon turning the light on after a period of 90 min. This result verifies the photocatalytic nature of the process.

Regarding the reaction intermediates identified in solution, results of GC/MS analysis showed that the main reaction product was acetone. The concentration of this compound was relatively high (5.5 mM) at t = 2 h and decreased progressively with irradiation time until it almost disappeared at t = 70 h. Other reaction products detected in much lower concentrations include acetaldehyde, which was present in the samples collected at t = 24–30 h, and formaldehyde, which was the only reaction product detected in small quantities at t = 70 h. As discussed in detail in our previous study of glycerol photo-reforming reaction over Pt/TiO_2 catalysts [73], these intermediates can be formed via a series of transformation steps that involve hydrogenolysis and/or dehydration of glycerol followed by dehydration, dehydrogenation and decarbonylation reactions. It is of interest to note, however, that both the nature and concentration of reaction intermediates in solution depend appreciably on the nature of the co-catalyst employed (i.e., Pt or CuO_x).

4. Conclusions

Copper-loaded TiO_2 photocatalysts with variable metal loading (0.01–2.8 wt.% Cu) have been synthesized employing the equilibrium deposition filtration (EDF) method. Results of photocatalyst characterization showed that the EDF method results in the formation of highly dispersed Cu(II) species, which interact strongly with the TiO_2 surface and retain their characteristics following calcination at 450 °C. The synthesized samples were found to be very active for the glycerol photo-reforming reaction toward H_2 and CO_2, which proceeds with intermediate formation of acetone, acetaldehyde and formic acid. The reaction rate increases significantly with increase of Cu loading up to *ca.* 1.0 wt.% Cu and is enhanced by a factor of 10 with increase of initial glycerol concentration from 0.37 mM to 1 M. Although bulk copper oxides are known to be unstable under photoreaction conditions, the present CuO_x/TiO_2 photocatalysts showed very good stability for the title reaction for initial glycerol concentrations higher than 10 mM. The hysteresis in hydrogen production as well as the rate fluctuations observed for H_2 and CO_2 evolution at low initial glycerol concentrations in solution have been attributed to a slow and reversible modification of the oxidation state of copper due to cyclic reduction/oxidation of dispersed CuO_x species by photogenerated electrons/holes. To our knowledge, this is the first example of a photocatalytic system that exhibits such dynamic characteristics.

Investigation of the oscillating behavior of the glycerol photo-reforming reaction rate could be very interesting both for the singularity of the phenomenon and for its potential contribution to reveal the quite unique characteristics of copper in photocatalytic systems. For this, an *in situ* technique able to monitor the phase composition of dispersed copper species with time-under-irradiation is necessary.

Acknowledgements

This research has been co-financed by the European Union (European Social Fund ESF) and Greek National Funds through the Operational Program "Education and Lifelong Learning" of the National Strategic Reference Framework (NSRF)—Research Funding Program: Thales. Investing in knowledge society through the European Social Fund (PhotoFuelCell project).

References

[1] P.D. Tran, L.H. Wong, J. Barber, J.S.C. Loo, Energy Environ. Sci. 5 (2012) 5902–5918.
[2] A. Kudo, Y. Miseki, Chem. Soc. Rev. 38 (2009) 253–278.
[3] M. Woodhouse, B.A. Parkinson, Chem. Soc. Rev. 38 (2009) 197–210.
[4] K. Maeda, J. Photochem. Photobiol. C 12 (2011) 237–268.
[5] A. Fujishima, K. Honda, Nature 238 (1972) 37–38.
[6] J.R. Bolton, Solar Energy 57 (1996) 37–50.
[7] M. Graetzel, Nature 414 (2001) 338–344.
[8] T. Bak, J. Nowotny, M. Rekas, C.C. Sorrell, Int. J. Hydrogen Energy 27 (2002) 991–1022.
[9] X. Chen, S. Shen, L. Guo, S.S. Mao, Chem. Rev. 110 (2010) 6503–6570.
[10] T. Kawai, T. Sakata, Nature 286 (1980) 474–476.
[11] M. Kawai, T. Kawai, K. Tamaru, Chem. Lett. 8 (1981) 1185–1188.
[12] A. Patsoura, D.I. Kondarides, X.E. Verykios, Catal. Today 124 (2007) 94–102.
[13] D.I. Kondarides, V.M. Daskalaki, A. Patsoura, X.E. Verykios, Catal. Lett. 122 (2008) 26–32.
[14] V.M. Daskalaki, D.I. Kondarides, Catal. Today 144 (2009) 75–80.
[15] G.L. Chiarello, D. Ferri, E. Selli, J. Catal. 280 (2011) 168–177.
[16] M. Cargnello, A. Gasparotto, V. Gombac, T. Montini, D. Barreca, P. Fornasiero, Eur. J. Inorg. Chem. (2011) 4309–4323.
[17] H. Bahruji, M. Bowker, P.R. Davies, F. Pedrono, Appl. Catal. B 107 (2011) 205–209.
[18] O. Carp, C.L. Huisman, A. Reller, Prog. Solid State Chem. 32 (2004) 33–177.
[19] D. Duonghong, E. Borgarello, M. Grätzel, J. Am. Chem. Soc. 103 (1981) 4685–4690.
[20] A.J. Bard, J. Phys. Chem. 86 (1982) 172–177.
[21] A.L. Linsebigler, G. Lu, J.T. Yates Jr., Chem. Rev. 95 (1995) 735–758.
[22] P.V. Kamat, J. Phys. Chem. Lett. 3 (2012) 663–672.
[23] V. Gombac, L. Sordelli, T. Montini, J.J. Delgado, A. Adamski, G. Adami, M. Cargnello, S. Bernal, P. Fornasiero, J. Phys. Chem. A 114 (2010) 3916–3925.
[24] A.V. Korzhak, N.I. Ermokhina, A.L. Stroyuk, V.K. Bukhtiyarov, A.E. Raevskaya, V.I. Litvin, S.Ya. Kuchmiy, V.G. Ilyin, P.A. Manorik, J. Photochem. Photobiol. A 198 (2008) 126–134.
[25] M. Sahu, P. Biswas, Nanoscale Res. Lett. 6 (2011) 441.
[26] B. Choudhury, M. Dey, A. Choudhury, Int. Nano Lett. 3 (2013) 1–8.
[27] A.O. Musa, T. Akomolafe, M.J. Carter, Solar Energy Mater. Solar Cells 51 (1998) 305–316.
[28] M. Nolan, S.D. Elliott, Phys. Chem. Chem. Phys. 8 (2006) 5350–5358.
[29] K.L. Hardee, A.J. Bard, J. Electrochem. Soc. 124 (1977) 215–224.
[30] W. Siripala, A. Ivanovskaya, T.F. Jaramillo, S.-H. Baeck, E.W. McFarland, Sol. Energy Mater. Sol. Cells 77 (2003) 229–237.
[31] G.K. Mor, O.K. Varghese, R.H.T. Wilke, S. Sharma, K. Shankar, T.J. Latempa, K.-S. Choi, C.A. Grimes, Nano Lett. 8 (2008) 1906–1911.
[32] J. Arana, C. Fernandez Rodriguez, O. Gonzalez Diaz, J.A. Herrera Melian, J. Perez Pena, Catal. Today 101 (2005) 261–266.
[33] G. Li, N.M. Dimitrijevic, L. Chen, T. Rajh, K.A. Gray, J. Phys. Chem. C 112 (2008) 19040–19044.
[34] H. Irie, S. Miura, K. Kamiya, K. Hashimoto, Chem. Phys. Lett. 457 (2008) 202–205.
[35] M. Liu, X. Qiu, M. Miyauchi, K. Hashimoto, Chem. Mater. 23 (2011) 5582–5586.
[36] L. Liu, X. Gu, C. Sun, H. Li, Y. Deng, F. Gao, L. Dong, Nanoscale 4 (2012) 6351–6359.
[37] G.S. Pozan, M. Isleyen, S. Gokcen, Appl. Catal. B 140–141 (2013) 537–545.
[38] N.-L. Wu, M.-S. Lee, Int. J. Hydrogen Energy 29 (2004) 1601–1605.
[39] J. Bandara, C.P.K. Udawatta, C.S.K. Rajapakse, Photochem. Photobiol. Sci. 4 (2005) 857–861.
[40] H.-J. Choi, M. Kang, Int. J. Hydrogen Energy 32 (2007) 3841–3848.
[41] D. Barreca, P. Fornasiero, A. Gasparotto, V. Gombac, C. Maccato, T. Montini, E. Tondello, Chemsuschem 2 (2009) 230–233.
[42] S.S. Lee, H. Bai, Z. Liu, D.D. Sun, Water Res. 47 (2013) 4059–4073.
[43] K.B. Dhanalakshmi, S. Latha, S. Anandan, P. Maruthamuthu, Int. J. Hydrogen Energy 26 (2001) 669–674.
[44] T. Sreethawong, S. Yoshikawa, Catal. Commun. 6 (2005) 661–668.
[45] B.A. Andersson, Prog. Photovolt. Res. Appl. 8 (2000) 61–76.
[46] D. Barreca, A. Gasparotto, C. Maccato, E. Tondello, O.I. Lebedev, G. Van Tendeloo, Cryst. Growth Des. 9 (2009) 2470–2480.
[47] D. Barreca, G. Carraro, A. Gasparotto, C. Maccato, O.I. Lebedev, A. Parfenova, S. Turner, E. Tondello, G. Van Tendeloo, Langmuir 27 (2011) 6409–6417.
[48] D. Barreca, G. Carraro, E. Comini, A. Gasparotto, C. Maccato, C. Sada, G. Sberveglieri, E. Tondello, J. Phys. Chem. C 115 (2011) 10510–10517.
[49] K.C.C Kharas, Appl. Catal. B 2 (1993) 207–224.
[50] A. Dandekar, M.A. Vannice, Appl. Catal. B 22 (1999) 179–200.
[51] R. Zhou, T. Yu, X. Jiang, F. Chen, X. Zheng, Appl. Surf. Sci. 148 (1999) 263–270.
[52] J. Ramirez-Ortiz, T. Ogura, J. Medina-Valtierra, S.E. Acosta-Ortiz, P. Bosch, J.A. de los Reyes, V.H. Lara, Appl. Surf. Sci. 174 (2001) 177–184.
[53] A. Balian, G. Hatzigiannis, D. Eng, M. Stoukides, J. Catal. 145 (1994) 526–536.
[54] I. Böttger, T. Schedel-Niedrig, O. Timpe, R. Gottschall, M. Hävecker, T. Ressler, R. Schlögl, Chem. Eur. J. 6 (2000) 1870–1876.
[55] T. Ochs, T. Turek, Chem. Eng. Sci. 54 (1999) 4513–4520.
[56] O.V. Komova, A.V. Simakov, V.A. Rogov, D.I. Kochubei, G.V. Odegova, V.V. Kriventsov, E.A. Paukshtis, V.A. Ushakov, N.N. Sazonova, T.A. Nikoro, J. Mol. Catal. A 161 (2000) 191–204.
[57] A. Amariglio, O. Benali, H. Amariglio, J. Catal. 118 (1989) 164–174.
[58] H. Werner, D. Herein, G. Schulz, U. Wild, R. Schlögl, Catal. Lett. 49 (1997) 109–119.
[59] A. Knop-Gericke, M. Hävecker, T. Schedel-Niedrig, R. Schlögl, Top. Catal. 15 (2001) 27–34.
[60] B. Zhou, Z. Liu, H. Wang, Y. Yang, W. Su, Catal. Lett. 132 (2009) 75–80.
[61] C. Contiu, J. Berg, A. Drochner, H. Vogel, R. von Watzdorf, Catal. Today 157 (2010) 231–235.
[62] F.J.R. van Neer, B. van der Linden, A. Bliek, Catal. Today 38 (1997) 115–128.
[63] J. Tsou, P. Magnoux, M. Guisnet, J.J.M. Orfao, J.L. Figueiredo, J. Catal. 225 (2004) 147–154.
[64] P. Ciambelli, A. Di Benedetto, R. Pirone, G. Russo, Chem. Eng. Sci. 54 (1999) 2555–2559.
[65] M. Orban, K. Kurin-Csorgei, G. Rabai, I.R. Epstein, Chem. Eng. Sci. 55 (2000) 267–273.
[66] C. Wagner, Ber. Bunsenges. Phys. Chem. 74 (1970) 401.
[67] H. Bluhm, M. Hävecker, A. Knop-Gericke, E. Kleimenov, R. Schlö1gl, D. Teschner, V.I. Bukhtiyarov, D.F. Ogletree, M. Salmeron, J. Phys. Chem. B 108 (2004) 14340–14347.
[68] M. Greger, B. Ihme, M. Kotter, L. Riekert, Ber. Bunsenges. Phys. Chem. 88 (1984) 427–433.
[69] G.D. Panagiotou, T. Petsi, K. Bourikas, C.S. Garoufalis, A. Tsevis, N. Spanos, C. Kordulis, A. Lycourghiotis, Adv. Colloid Interface Sci. 142 (2008) 20–42.
[70] R.A. Spurr, H. Myers, Anal. Chem. 59 (1957) 760–762.
[71] B.D. Cullity, 'Elements of X-Ray Diffraction, Addison-Wesley Publishing Company, Inc., Reading, MA, 1956.
[72] A. Patsoura, D.I. Kondarides, X.E. Verykios, Appl. Catal. B 64 (2006) 171–179.
[73] P. Panagiotopoulou, E.E. Karamerou, D.I. Kondarides, Catal. Today 209 (2013) 91–98.
[74] G.N. Nomikos, P. Panagiotopoulou, D.I. Kondarides, X.E. Verykios, Appl. Catal. B 146 (2014) 249–257.
[75] H. Praliaud, S. Mikhailenko, Z. Chajar, M. Primet, Appl. Catal. B 16 (1998) 359–374.
[76] G. Colón, M. Maicu, M.C. Hidalgo, J.A. Navío, Appl. Catal. B 67 (2006) 41–51.
[77] J. Vakros, K. Bourikas, S. Perlepes, Ch. Kordulis, A. Lycourghiotis, Langmuir 20 (2004) 10542–10550.
[78] Th. Petsi, G.D. Panagiotou, Ch.S. Garoufalis, Ch. Kordulis, P. Stathi, Y. Deligiannakis, A. Lycourghiotis, K. Bourikas, Chem. Eur. J. 15 (2009) 13090–13104.
[79] K. Bourikas, J. Stavropoulos, C.S. Garoufalis, Ch. Kordulis, Th. Petsi, A. Lycourghiotis, Chem. Eur. J. 17 (2011) 1201–1213.
[80] L. Espinosa-Alonso, K.P. de Jong, B.M. Weckhuysen, J. Phys. Chem. C 112 (2008) 7201–7209.
[81] L. Espinosa-Alonso, A.A. Lysova, P. de Peinder, K.P. de Jong, I.V. Koptyug, B.M. Weckhuysen, J. Am. Chem. Soc. 131 (2009) 6525–6534.
[82] P. Malet, A. Munoz-Paez, C. Martin, J. Catal. 134 (1992) 47–57.
[83] K. Bourikas, Ch. Fountzoula, Ch. Kordulis, Appl. Catal. B 52 (2004) 145–153.
[84] K. Bourikas, Ch. Fountzoula, Ch. Kordulis, Langmuir 20 (2004) 10663–10669.
[85] R.M. Friedman, J.J. Freeman, F.W. Lytle, J. Catal. 55 (1978) 10–28.
[86] M.K.I. Senevirathna, P.K.D.D.P. Pitigala, K. Tennakone, J. Photochem. Photobiol. A 171 (2005) 257–259.
[87] H.W. Slamet, E. Nasution, S. Purnama, J. Kosela, Gunlazuardi, Catal. Commun. 6 (2005) 313–319.
[88] A. Mills, S.-K. Lee, Platinum Met. Rev. 47 (2003) 2–12.
[89] N. Helaïli, Y. Bessekhouad, A. Bouguelia, M. Trari, J. Hazard. Mater. 168 (2009) 484–492.
[90] P.E. de Jongh, D. Vanmaekelbergh, J.J. Kelly, Chem. Commun. (1999) 1069–1070.
[91] Y. Bessekhouad, D. Robert, J.-V. Weber, Catal. Today 101 (2005) 315–321.
[92] L. Huang, F. Peng, H. Yu, H. Wang, Solid State Sci. 11 (2009) 129–138.
[93] D. Zhang, F. Zeng, Russ. J. Phys. Chem. 85 (2011) 1077–1083.
[94] Y.-H. Xu, D.-H. Liang, M.-L. Liu, D.-Z. Liu, Mater. Res. Bull. 43 (2008) 3474–3482.